Article

INTERNATIONAL JOURNAL OF DAMAGE MECHANICS

International Journal of Damage Mechanics
2017, Vol. 26(6) 919–932

DOI: 10.1177/1056789516635727
journals.sagepub.com/home/ijd
SAGE

Fatigue damage propagation models for ductile fracture of ultrahigh toughness cementitious composites

Wen Liu[1], Shilang Xu[2] and Peng Feng[3]

Abstract

Ultrahigh toughness cementitious composites are a kind of high-performance cementitious material with a characteristic of ductile fracture. Based on the continuum damage mechanics theory and flexural fatigue damage model, two damage propagation models of ultrahigh toughness cementitious composites are built. One is a linear bilogarithmic model with *J*-integral range as its independent variable, while the other one is a linear model on a semilogarithmic scale with fatigue stress level as its independent variable. However, according to former research, the *J*-integral depends strongly on specimens' geometry, so the first damage propagation model is deeply influenced by material dimension. As a result, the second damage propagation model is more convenient in application, shows the material fatigue property in comparison with the first model. In order to prove these two models and obtain the parameters, a three-point flexural fatigue experiment on single-edge-notched fracture specimens is carried out. The results shows that the two models fit better with the experimental results, rather than the crack propagation law of ultrahigh toughness cementitious composites.

Keywords

Ultrahigh toughness cementitious composites, ductile fracture, damage propagation model, *J*-integral, stress level

Introduction

Ultrahigh toughness cementitious composites (UHTCC), which has another name as engineering cementitious composites (ECC), is a kind of short fiber reinforced cementitious composites. This material has the characteristics of pseudo strain hardening and multiple cracking under uniaxial

[1]Department of Civil Engineering, Beijing Forestry University, Beijing, China
[2]Institute of Advanced Engineering Structures and Materials, Zhejiang University, Hangzhou, China
[3]Department of Civil Engineering, Tsinghua University, Beijing, China

Corresponding author:
Wen Liu, Beijing Forestry University, Qinghua Dong Road, Beijing 100083, China.
Email: liuwen@bjfu.edu.cn

tensile load. Different from concrete's quasi-brittle fracture, "ductile fracture" happens for UHTCC (Li and Hashida, 1993). The total composite fracture energy can be divided into two parts: an off-crack-plane matrix-cracking component and an on-crack-plane fiber-bridging component. Maalej et al. (1995) took an experimental study on the effect of fiber volume fraction on the off-crack-plane fracture energy of ECC. The results showed that the off-crack-plane fracture energy increased with fiber volume fractions in a logarithmic fashion, and it exceeded the bridging fracture energy produced on the main fracture plane. Kabele and Horii proposed a simple analytical model for fracture analysis of ECC. In their research, ECC was idealized as a homogeneous and continuous, while a discrete crack model was applied for localized cracks (Kabele and Horii, 1996). Kabele and Li (1998) emphasized the off-crack-plane fracture energy and calculated the composite fracture energy of ECC with a finite element analysis on crack growth under small-scale yielding conditions. These above investigations are all based on the J-integral approach in nonlinear fracture mechanics. However, this approach has some limitations though it is widely applied in industry and engineering fields (Besson, 2010; Rice, 1968). For example, the J-integral is not a material intrinsic parameter because that it strongly depends on specimen's geometry (Sumpter and Forbes, 1992). Then, there is another approach called "Local Approach to Fracture," which is based on continuum damage mechanics (CDM). Many works have been devoted to investigate the damage fracture behavior of ductile solids since the CDM method was first introduced to solve the creep problem by Kachanov (1958). In the late 1980s, some researchers extended the damage concept for ductile plasticity (Ju, 1989; Lemaitre, 1984; Simo and Ju, 1987a, 1987b). Various isotropic and anisotropic damage models for ductile fracture in metal materials were built (Bonora, 1997; Chanderakanth and Pandey, 1995; Chow and Wang, 1987; Lemaitre, 1985; Tai and Yang, 1986, 1987; Wang, 1992a, 1992b). Besides, damage mechanics was also applied to predict the fatigue life of metal materials (Chaboche, 1998a, 1998b).

Based on nonlinear fracture mechanics, the authors introduced a double J-integral criterion to calculate the fracture energy of UHTCC (Liu et al., 2012). The J_R resistance curve could be used to evaluate the cracking state. According to this double J fracture model, a fatigue crack propagation law of UHTCC was built, which was similar to Paris law. This crack propagation law was expressed with the two parameters as J-integral and crack covering area (Xu and Liu, 2012). The fatigue property of UHTCC was also investigated, with an introduced flexural fatigue damage model on basis of CDM (Xu et al., 2013). Furthermore, on the base of these fracture and fatigue models, the damage property of UHTCC-concrete composite beam under flexural fatigue was researched (Liu et al., 2013). However, these investigations before mostly focused on the fracture energy of UHTCC. In this study, the CDM method is applied to analyze the damage propagation law during the fracture fatigue process of UHTCC. The damage propagation models are built, while a three-point flexural test on single-edge-notched fracture specimens is taken to calculate the parameters.

Continuum damage model for UHTCC fracture

Fatigue damage model of UHTCC

The fatigue damage model in this paper is constructed according to Chaboche fatigue damage model (Chaboche, 1981), as follows

$$\frac{\partial D}{\partial N} = [1 - (1 - D)^{1+\beta}]^{\alpha(Sm,S)} \left[\frac{S_a}{M(S_m)(1 - D)} \right]^{\beta} \tag{1}$$

where $S_m = \sigma_m/\sigma_u = (\sigma_{\max} + \sigma_{\min})/2\sigma_u$, $S_a = \sigma_a/\sigma_u$, while $\sigma_{\max}$ and $\sigma_{\min}$ are the maximum and minimum load during a fatigue cycle, σ_a and σ_m are the amplitude and the mean value of the fatigue stresses, σ_u is the ultimate static strength. D represents the fatigue damage; N is the number of load cycles; β is a material constant; $\alpha(S_m, S)$ and $M(S_m)$ are material functions determined by the shape of fatigue load. It is assumed that the fatigue damage begins to develop in the first load cycle, equation (1) is integrated with $D = 0 \sim 1$ and $N = 0 \sim N_F$, that is

$$N_F(S_m, S) = \frac{1}{(1-\alpha)(1+\beta)}\left[\frac{S_a}{M(S_m)}\right]^{-\beta} \tag{2}$$

$$D = 1 - \left[1 - \left(\frac{N}{N_F}\right)^{\frac{1}{1-\alpha}}\right]^{\frac{1}{1+\beta}} \tag{3}$$

in which, N_F represents the fatigue life. However, for equation (1), it is rather difficult to determine $\alpha(S_m, S)$ and $M(S_m)$. As a result, some simplified models are introduced, such as the modified Chaboche model by Wang (1992), as follows

$$\frac{\partial D}{\partial N} = (1-D)^{-\gamma}\left[\frac{\sigma_a}{2B(1-D)}\right]^{\beta} \tag{4}$$

where B, β, and γ are material parameters related with the environmental temperature, while B is also dependent on the average stress, as $B = B(\sigma_m)$. This simplified model is used in this study.

Compared with equation (1), equation (4) could be expressed as

$$\frac{\partial D}{\partial N} = (1-D)^{\alpha(\sigma_m,\sigma_{\max})}\left[\frac{\sigma_a}{M(\sigma_m)}\right]^{\beta} \tag{5}$$

The upper and lower integral limits of equation (5) are $D\big|_{N=N_s} = D_s$ and $D\big|_{N=N_F} = 1$, where D_s represents a starting value of fatigue damage, and N_s is the number of cycles when D equaled to D_s. Through integrating, the following equation is derived, as follows

$$\begin{aligned} \int_{D_s}^{D}(1-D)^{-\alpha(\sigma_M,\sigma_{\max})}dD = \int_{N_s}^{N}\left[\frac{\sigma_a}{M(\sigma_m)}\right]^{\beta}dN \to (1-D_s)^{1-\alpha(\sigma_m,\sigma_{\max})} - (1-D)^{1-\alpha(\sigma_m,\sigma_{\max})} \\ = [1-\alpha(\sigma_m,\sigma_{\max})]\left(\frac{\sigma_a}{M(\sigma_m)}\right)^{\beta}(N-N_s) \end{aligned} \tag{6}$$

Taking $D = 1$ and $N = N_F$ into the above equation, and it is written as

$$N_F - N_s = \frac{(1-D_s)^{1-\alpha(\sigma_m,\sigma_{\max})}}{1-\alpha(\sigma_m,\sigma_{\max})}\left(\frac{\sigma_a}{M(\sigma_m)}\right)^{-\beta} \tag{7}$$

Equation (7) is simplified with equation (4), as well as that σ_a and σ_m are considered as the function of stress level, the following model is obtained (Liu et al., 2014)

$$D = 1 - (1 - D_s)\left[1 - \frac{N/N_F - N_s/N_F}{1 - N_s/N_F}\right]^{\gamma(S)} \tag{8}$$

The exponent $\gamma(S)$ represents the damage cumulative degree. For UHTCC, the starting damage value, D_s, is taken as the initial damage of fatigue stage II. The parameters D_s and $\gamma(S)$ of UHTCC are obtained with stress level as follows

$$D_s = \begin{Bmatrix} 0.1696 & S \geq 0.90 \\ -0.3418 + 0.8102 \cdot S & S < 0.90 \end{Bmatrix} \tag{9}$$

$$\gamma(S) = 1.0879 S^{2.2861} \tag{10}$$

Damage propagation model of UHTCC

A ductile phenomenon happens during the fatigue damage process of UHTCC. In analyzing, this material is considered as an isotropic material due to the random distribution of PVA fibers. According to former research (Xu and Liu, 2012), the crack covering area, A, can be used as the parameter to describe the crack propagation law of UHTCC, as follows

$$\frac{\mathrm{d}A}{\mathrm{d}N} = C(\Delta J)^m \tag{11}$$

in which, ΔJ is the J-integral range during a fatigue cycle, while C and m are materials constants. During the fracture fatigue process, the irreversible parameter, fatigue cracking area, A, reflects the damage evolution with load cycles. Based on the former investigations on CMD model for ductile fracture (Chow and Wang, 1987; Wang, 1992b), the damage for ductile fracture can be similarly calculated by the following two common methods

$$D = D_0 + (D_c - D_0)\frac{(A - A_0)^\alpha}{(A_c - A_0)^\alpha} \tag{12}$$

$$D = D_0 + (D_c - D_0)\left\{1 - \left[1 - \frac{\ln(A/A_0)^\alpha}{\ln(A_c/A_0)^\alpha}\right]\right\} \tag{13}$$

where D_0, D_c, A_0, and A_c are the boundary conditions of fatigue damage and crack covering area. They are defined as

$$\begin{array}{lll} D = D_0 & \text{when} & A < A_0 \\ D = D_c & \text{when} & A = A_c \end{array} \tag{14}$$

According to equations (12) to (14), there exists a monotonous relation between fatigue damage and cracking area. Therefore, a damage propagation model similar to equation (11) can be deduced, as the following equation

$$\frac{\mathrm{d}D}{\mathrm{d}N} = c(\Delta J)^n \tag{15}$$

In this equation, c and n are material constants. Taking logarithm on both sides of equation (15), the following equation is obtained

$$\log\left(\frac{\mathrm{d}D}{\mathrm{d}N}\right) = \log c + n\log(\Delta J) \tag{16}$$

However, as stated in "Introduction" section, the parameter, J-integral, is not a material intrinsic parameter while it strongly depends on specimen geometry. In order to calculate the damage propagation rate accurately, an independent variable, the stress level S, is applied to describe the damage propagation. According to former research (Chaboche, 1988b; Wang, 1992), there exists an exponent relation between J-integral and maximum fatigue load as well as the fatigue stress level. Therefore, different from the bilogarithmic linear relation shown in equation (16), a semilogarithmic relation exists between damage propagation rate and stress level, as follows

$$\log\left(\frac{\mathrm{d}D}{\mathrm{d}N}\right) = a + b \cdot S \tag{17}$$

where a and b are material constants. In this study, a fatigue experiment on fracture specimens is carried out to prove equations (16) and (17), as well as to obtain the parameters.

Fatigue experiment of single-edge-notched fracture specimen

Experiment program

A three-point flexural experiment is taken on single-edge-notched fracture specimens of UHTCC. Specimens are produced with cementitious binders, fine sand, water, super plasticizer, and polyvinyl alcohol (PVA) fiber. The corresponding volume fraction of PVA fiber in UHTCC is set as 2.0%. The dimension of all specimens is $400\,\mathrm{mm} \times 100\,\mathrm{mm} \times 100\,\mathrm{mm}$. After standard cure for 28 days, the specimens are laid in the indoor environment for three months. Before test, a single edge notch is cut with a depth of 40 mm.

All specimens are loaded by a 250 kN MTS testing machine. For fatigue test, fatigue load of constant amplitude is adopted, with a sinusoidal control of 5 Hz. The maximum and minimum fatigue loads are determined according to the average ultimate loads of static specimens, as shown in Table 1. The experimental setup is shown in Figure 1. The support span is 300 mm, with the load applied vertically at the midpoint. Two π gauges are employed to measure the crack tip opening displacement and crack mouth opening displacement (CMOD). One linear variable differential transducer is used to measure the midspan deflection. The crack covering area is monitored with a large number of square grids labeled in front of the notch tip on the side surface. Grids with a length of 1 mm are adopted, while the area for each grid is $1\,\mathrm{mm}^2$. The cracking area equals to the total area of the square elements which are crossed by the cracks.

Table 1. Fatigue loads and corresponding stress levels.

Ultimate static load (P_u/kN)	Specimen no.	Maximum load (P_{max}/kN)	Minimum load (P_{min}/kN)	Mean load (P_m/kN)	Amplitude (P_a/kN)	Stress level (S)
8.42	F2.0-1	7.5	1.5	4.5	3	0.890
	F2.0-2	7	1	4	3	0.831
	F2.0-3	6.5	1.5	4	2.5	0.771
	F2.0-4	6	1	3.5	2.5	0.712
	F2.0-5	6	1.5	3.75	2.25	0.712
	F2.0-6	5.5	1.5	3.5	2	0.653

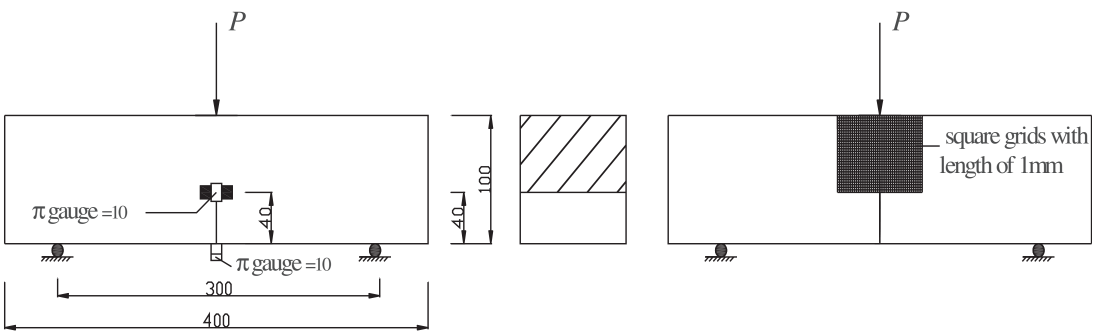

Figure 1. Test setup and measuring method /mm.

Experiment result

During the test, multiple cracks are generated for all fatigue specimens, emerging at the notch tip and propagating toward the loading point. The number of fatigue cracks reduces with the decrease of fatigue stress level. Figure 2 displays the evolution curves of maximum CMOD with the load cyclic ratio and the load cyclic number. As is seen in this diagram, the deformation capability declines with the decrease of fatigue stress levels due to fewer cracks. Three stages exist during the deformation process: I, rapid developing stage, II, stable developing stage, and III, failure stage. These three stages take up about 5, 75–85, and 10–20% of the fatigue life, respectively. For specimen F2.0-6, it is found that the maximum CMOD develops constantly in the later period and no localized crack emerges. It is regarded that fatigue failure would not happen for this specimen, because that the fracture energy produced by the fatigue loads on specimen F2.0-6 is below its fatigue threshold.

Crack propagation law of UHTCC

Figure 3 shows the evolution curves of fatigue cracking area with cyclic ratio. A similar three-stage developing trend exists. In equation (11), the average rate of crack growth during the fatigue life is used to calculate the formula parameters. As a result, the more even of the crack propagation rate, the more accurate of the computed results. Therefore, only the crack propagation rate in stage II is

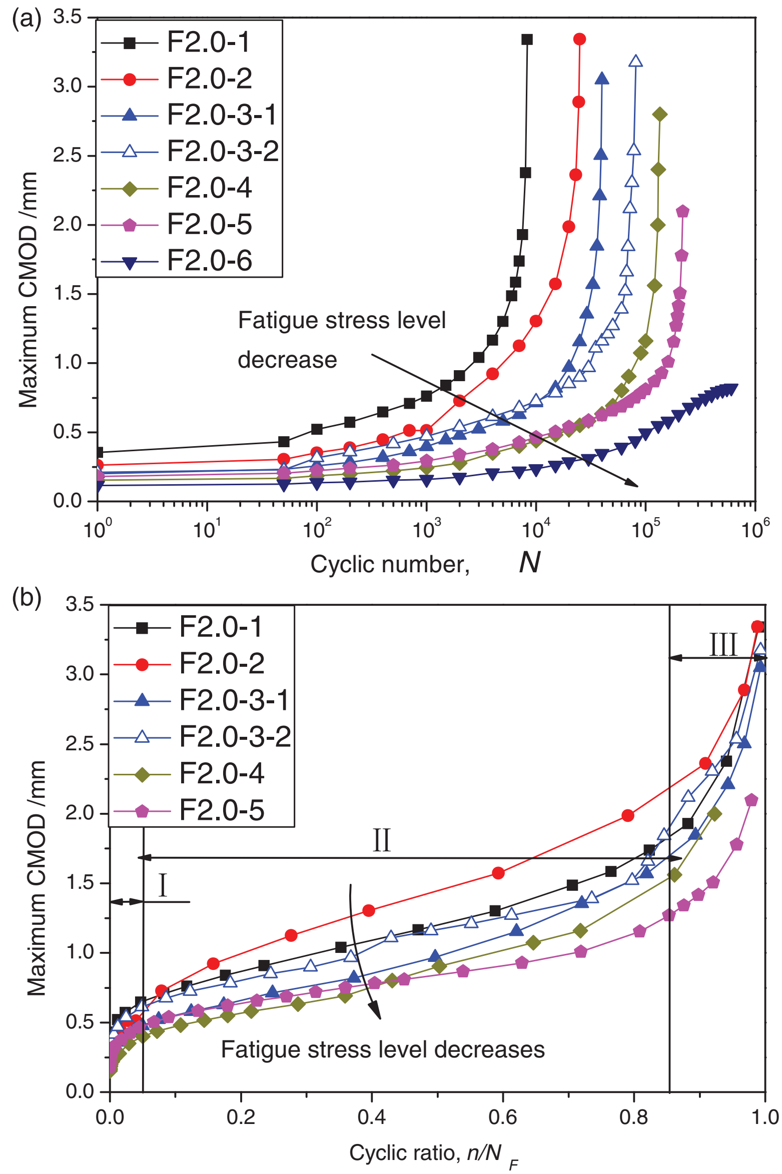

Figure 2. Evolution curves of maximum CMOD with cyclic ratio and cyclic number. (a) CMOD $\sim N$, (b) CMOD $\sim N/N_F$.

considered in this study. Take logarithm on both sides of equation (11), then the following equation is obtained

$$\log\left(\frac{\mathrm{d}A}{\mathrm{d}N}\right) = \log C + m \log(\Delta J) \tag{18}$$

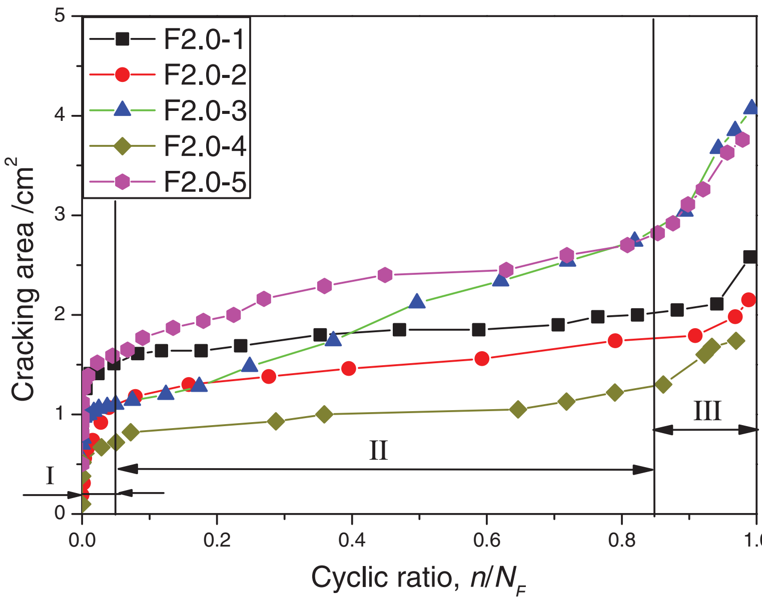

Figure 3. Evolution curves of cracking area with cyclic ratio.

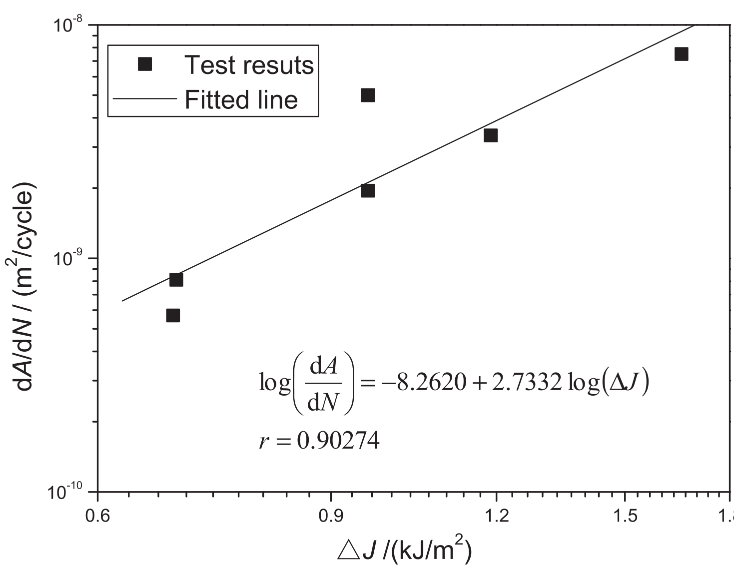

Figure 4. Fitted linear bilogarithmic relation between crack propagation rate and J-integral amplitude.

Taking $\log(dA/dN)$ and $\log(\triangle J)$ as the vertical and horizontal ordinates, respectively, the calculated results are plotted in this coordinate, as shown in Figure 4. A linear relation is fitted between the two variables, with the correlation coefficient $r = 0.90275$. From this fitted line in this graph, the parameters in equation (12) are regressed as $C = 2.3659 \times 10^{-9}$ and $m = 2.7332$ (Liu et al., 2014; Xu and Liu, 2012).

Table 2. Experimental data and calculated results of the fatigue damage propagation rate.

Specimen no.	Test data						Calculated results		
	S	N_F	N_s	N_f	N_{II}	$\triangle J/(kJ/m^2)$	D_s	D_f	$dD/dN \times 10^{-6}$
F2.0-1	0.890	8501	425	7225	6801	1.647	0.38151	0.95661	84.5741
F2.0-2	0.831	25,301	1265	21,505	20,241	1.184	0.33272	0.93074	29.5463
F2.0-3-1	0.771	40,285	2014	34,242	32,228	0.952	0.28391	0.89377	18.9233
F2.0-3-2	0.771	81,586	4079	69,348	65,269	0.952	0.28391	0.89377	9.34380
F2.0-4	0.712	139,265	6963	118,375	111,412	0.684	0.23509	0.84326	5.45878
F2.0-5	0.712	222,657	11,133	189,258	178,126	0.680	0.23509	0.84326	3.41429

Fatigue damage propagation law of UHTCC

Fatigue damage calculation

Equations (8) to (10) are used to calculate the initial and final fatigue damages of stage II of single-edge-notched specimens. The boundaries of this stage are taken as 5 and 85%, respectively. The average values of damage propagation rate during fatigue stage II are computed, and the results are listed in Table 2. In this table, N_F and N_{II} represent the full fatigue life and the fatigue life of stage II, respectively; N_s and N_f are the initial and final load cycle numbers of stage II; D_s and D_f are the initial and final damage values of stage II, while $\triangle D$ is the damage propagation quantity in this stage; dD/dN is the average damage propagation rate. ΔJ is J-integral value amplitude of the fatigue test, which is determined by the static test.

Damage propagation model with J-integral

According to equation (16), taking $\log(dD/dN)$ and $\log(\triangle J)$ as the vertical and horizontal ordinates, respectively, the calculated results in Table 2 are shown in Figure 5. From this graph, a good linear relation exists between the two variables, with the correlation coefficient as $r = 0.97422$. Material constants in equation (16) are obtained as $c = 1.5878 \times 10^{-5}$ and $n = 3.3986$.

Because these two equations have the same independent viable, a comparison is taken between them. The results of them are shown in Figure 6, which shows the test results and the calculated exponential curves. The two curves in this figure have different vertical coordinates, one is dD/dN and another is dA/dN. As explained before, the dD/dN calculated curve, which reflects the first damage propagation model, is obtained according to the fatigue damage model (equation (8)), and only the experimental fatigue lives of the fracture specimens are used here. While for the dA/dN calculated curve, the experimental results of the fracture specimens, including fatigue lives and fatigue cracking area, are applied to compute the crack propagation model. From Figure 6, it is seen that these two curves develop similarly although they are calculated in two different ways. During smaller J-integral ranges, which means lower stress levels, a good fitness for the two curves is obtained. While at higher stress levels, it is obvious that the dD/dN curve fits better with the experimental data points than the dA/dN curve. Indeed it is seen that the dA/dN curve develops faster than the dD/dN curve in that it exceeds the experimental data points more and more. This is because that fatigue cracks develop faster at high stress level, and the observation error is obvious, while the dD/dN curve is calculated according to the fatigue damage model. As a result,

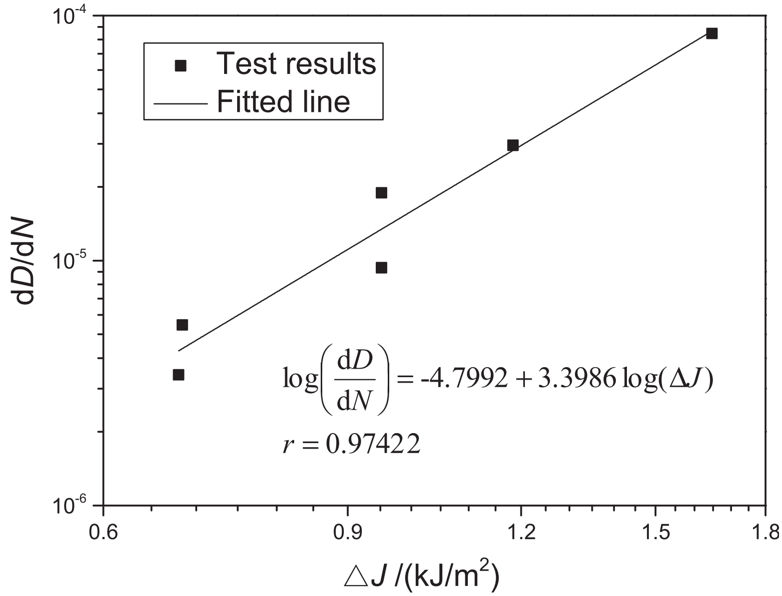

Figure 5. Bilogarithmic linear relation of damage propagation rate with J-integral range.

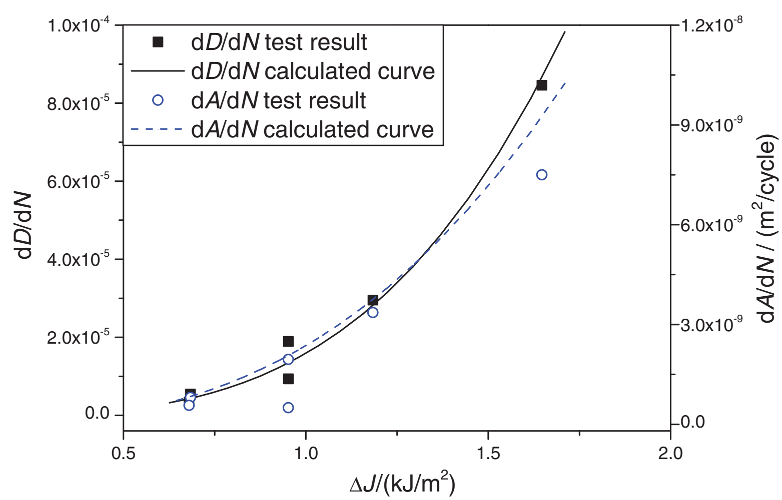

Figure 6. Comparison between damage propagation rate and crack propagation rate.

the $\mathrm{d}D/\mathrm{d}N$ model is more accurate in expressing the fatigue development rather than the $\mathrm{d}A/\mathrm{d}N$ model. Therefore, rather than the crack propagation law of equation (11), the damage propagation model of equation (15) is supposed to have a better effect in describing the fatigue process and damage develop of UHTCC, and the model parameters are $c = 1.5878 \times 10^{-5}$ and $n = 3.3986$.

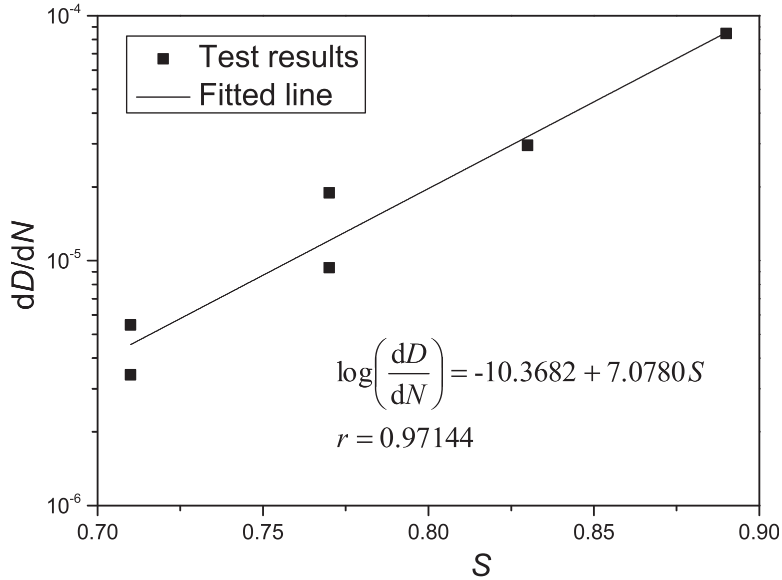

Figure 7. Semilogarithmic linear relation between damage propagation rate and stress level.

Damage propagation model with stress level

With the computed data in Table 2 and the fatigue stress levels of the fracture specimens, the calculated results of the second damage propagation model, equation (17), are shown in Figure 7. As is seen in this graph, there has been an obvious linear semilogarithmic phenomenon with the correlation coefficient $r = 0.97144$. Material constants in equation (17) are fitted as $a = -10.3682$ and $b = 7.0780$. Figure 8 shows the calculated curves of the two fatigue damage propagation models, equations (15) and (17), respectively. All these two models and the crack propagation model of equation (11) illustrate the fatigue propagation process of UHTCC. It is seen that the correlation coefficients of the two damage propagation model are $r = 0.97144$ and $r = 0.97422$, while this value for the crack propagation model is $r = 0.90274$. In another words, the two curves of the damage propagation models have good fitness with the test results, which means that the two models introduced in this study are more accurate than the crack propagation model. However, for these two models, the second one is better in application because that it is not affected by material geometry. Although the first damage propagation model is sensitive to specimen geometry, this model is introduced for the purpose of constructing a connection and a comparison with the fatigue crack propagation law, $\frac{dA}{dN} = C(\Delta J)^m$, which is similar to the Paris law (Xu and Liu, 2012). Another reason is that the J-integral is a parameter widely used in nonlinear fracture mechanics for ductile fracture, which is suitable for UHTCC.

Conclusions

Based on the CDM method, the fatigue damage propagation models of UHTCC are investigated through three-point flexural fatigue experiment on single-edge-notched fracture specimens. The continuum damage model of UHTCC under flexural fatigue is used to build the damage

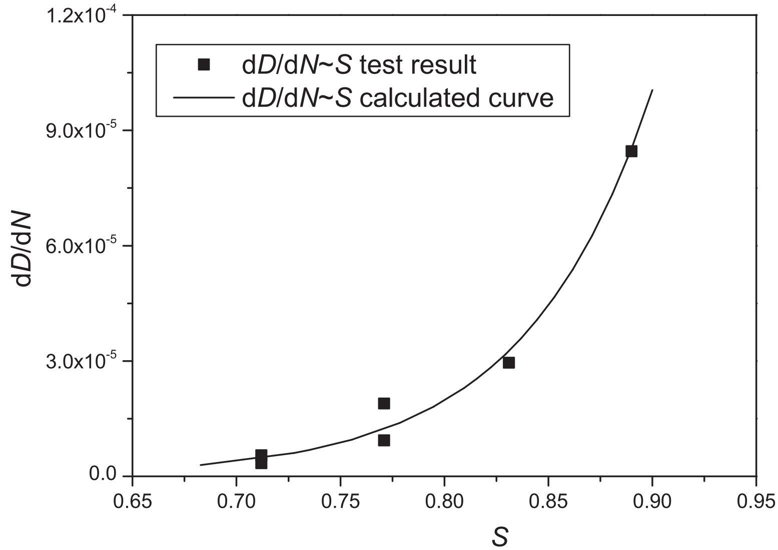

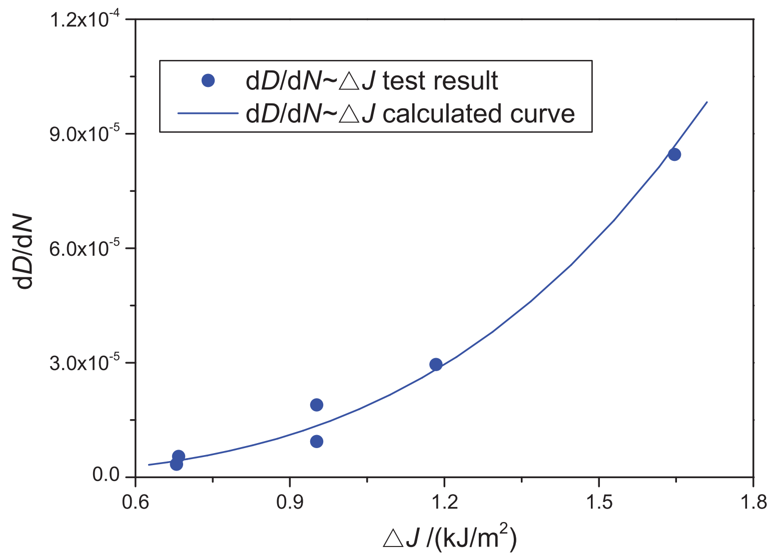

Figure 8. Calculated damage propagation rate. (a) dD/d$N \sim S$, (b) dD/d$N \sim \triangle J$.

propagation models. Two damage propagation models are introduced. For the first model, $\frac{\mathrm{d}D}{\mathrm{d}N} = c(\Delta J)^n$ with $c = 1.5878 \times 10^{-5}$ and $n = 3.3986$, it shows to fit better with the experimental results rather than the crack propagation model, $\frac{\mathrm{d}A}{\mathrm{d}N} = C(\Delta J)^m$ with $C = 2.3659 \times 10^{-9}$ and $m = 2.7332$. This model is introduced for the one purpose to construct a connection and a comparison with the fatigue crack propagation model, for another reason is that, the J-integral is parameter widely used in nonlinear fracture mechanics for ductile fracture of UHTCC. However, because that the independent variable in this model, $\triangle J$, depends strongly on specimen geometry, another model, a linear semilogarithmic equation, $\log\left(\frac{\mathrm{d}D}{\mathrm{d}N}\right) = a + b \cdot S$ with $a = -10.3682$ and $b = 7.0780$, is built to overcome the effect of specimen geometry. The second model also fits well with the test results. Furthermore, the fatigue stress level S of this second model is an independent parameter; it is only relevant with the load setting, thus is more convenient in application.

Declaration of Conflicting Interests

The author(s) declared no potential conflicts of interest with respect to the research, authorship, and/or publication of this article.

Funding

The author(s) disclosed receipt of the following financial support for the research, authorship, and/or publication of this article: The National Natural Science Foundation of China (Project 51308046) and the Open Fund Project of State Key Laboratory of Coastal and Offshore Engineering of Dalian University of Technology (No. LP1516).

References

Besson J (2010) Continuum models of ductile fracture: A review. *International Journal of Damage Mechanics* 19(1): 3–52.

Bonora N (1997) A nonlinear CDM model for ductile failure. *Engineering Fracture Mechanics* 58(1/2): 11–28.

Chaboche JL (1981) Continuous damage mechanics—A tool to describe phenomena before crack initiation. *Nuclear Engineering and Design* 64(2): 233–247.

Chaboche JL (1988a) Continuum damage mechanics part I—General concept. *Journal of Applied Mechanics* 55(1): 59–64.

Chaboche JL (1988b) Continuum damage mechanics part II—Damage growth, crack initiation and crack growth. *Journal of Applied Mechanics* 55(1): 65–72.

Chanderakanth S and Pandey PC (1995) An isotropic damage model for ductile material. *Engineering Fracture Mechanics* 50(4): 457–465.

Chow CL and Wang J (1987) An anisotropic theory continuum damage mechanics for ductile fracture. *Engineering Fracture Mechanics* 27(5): 547–558.

Ju JW (1989) On energy based coupled elastoplastic damage theories—Constitutive modelling and computational aspects. *International Journal of Solids and Structures* 25(7): 803–830.

Kabele P and Horii H (1996) Analysis model for fracture behaviors of pseudo strain-hardening cementitious composites. *Journal of Materials, Concrete and Structural Pavements* 30: 209–219.

Kabele P and Li VC (1998) Fracture energy of strain-hardening cementitious composites. In: *Fracture Mechanics of Concrete Structures*, *Proceedings FRAMCOS-3*. Freiburg: AEDIFICATIO Publishers, pp.487–498.

Kachanov LM (1958) Time of the rupture process under creep condition. *Izvestiya Akademii Nauk SSSR, Otdelenie Tekhnicheskikh Nauk* 8(8): 26–31.

Lemaitre J (1984) How to use damage mechanics. *Nuclear Engineering and Design* 80(2): 233–246.

Lemaitre J (1985) A continuum damage mechanics model for ductile fracture. *Journal of Engineering Materials and Technology* 107(1): 83–89.

Li VC and Hashida T (1993) Engineering ductile fracture in brittle-matrix composites. *Journal of Materials Science Letters* 12(12): 898–901.

Liu W, Xu SL and Li QH (2012) Experimental study on fracture performance of ultra-high toughness cementitious composites with J-integral. *Engineering Fracture Mechanics* 96: 656–666.

Liu W, Xu SL and Li QH (2013) Flexural behavior of UHTCC-layered concrete composite beam subjected to static and fatigue loads. *Fatigue and Fracture of Engineering Materials and Structures* 36(8): 738–749.

Liu W, Xu SL and Li HD (2014) Flexural fatigue damage model of ultra-high toughness cementitious composite. *International Journal of Damage Mechanics* 23(7): 949–963.

Maalej M, Hashida T and Li VC (1995) Effect of fiber volume fraction on the off-crack-plane fracture energy in strain-hardening engineered cementitious composites. *Journal of the American Ceramic Society* 78(12): 3369–3375.

Rice JR (1968) A path independent integral and approximate analysis of strain concentration by notched and cracks. *Journal of Applied Mechanics* 35(2): 379.

Simo JC and Ju JW (1987a) Strain and stress-based continuum damage mechanics model—I. Simulation. *International Journal of Solids and Structures* 23(7): 821–840.

Simo JC and Ju JW (1987b) Strain and stress-based continuum damage mechanics model—II. Computational aspects. *International Journal of Solids and Structures* 23(7): 841–846.

Sumpter JDG and Forbes AT (1992) Constraint based analysis of shallow cracks in mild stress. In: *1st International Conference on Shallow Crack Fracture Mechanics Toughness Tests and Applications*, Paper 7, pp.54–62, Cambridge, UK: The Welding Institute.

Tai WH and Yang BX (1986) A new microvoid-damage model for ductile fracture. *Engineering Fracture Mechanics* 25(3): 372–384.

Tai WH and Yang BH (1987) A new damage mechanics criterion for ductile fracture. *Engineering Fracture Mechanics* 27(4): 371–386.

Wang J (1992) Low cycle fatigue and cycle dependent creep with continuum mechanics. *International Journal of Damage Mechanics* 1(2): 237–244.

Wang TJ (1992a) Unified CDM model and local criterion for ductile fracture-I. Unified CDM model for ductile fracture. *Engineering Fracture Mechanics* 42(1): 177–183.

Wang TJ (1992b) Unified CDM model and local criterion for ductile fracture-II. Ductile fracture local criterion based on the CDM Model. *Engineering Fracture Mechanics* 42(1): 185–193.

Xu SL and Liu W (2012) Investigation on crack propagation law of ultra-high toughness cementitious composites under fatigue flexure. *Engineering Fracture Mechanics* 93: 1–12.

Xu SL, Liu W and Li QH (2013) Deformation calculation of ultra-high toughness cementitious composites-concrete beam under flexure with ultra-high toughness cementitious fatigue damage model. *International Journal of Damage Mechanics* 22(1): 116–132.